Journal of Engineering Science and Technology
Vol. 14, No. 5 (2019) 2928 - 2946
© School of Engineering, Taylor's University

EFFECT OF RESIDUAL STRESSES ON THE TI-6AL-4V CRUCIFORM SHAPE WELDED JOINTS BY XRD TECHNIQUE AND INFLUENCE OF HARDNESS - AN EXPERIMENT APPROACH

SRINIVASAREDDY VEMPATI[1,*],
K. VENKATA SUBBAIAH[2], K. BRAHMA RAJU[3]

[1]Department of Mechanical Engineering, QIS College of Engineering and Technology, Ongole, Andhra Pradesh, India
[2]Department of Mechanical Engineering, Andhra University, Visakhapatnam, Andhra Pradesh, India
[3]Department of Mechanical Engineering, SRKR Engineering College, Bhimavaram, Andhra Pradesh, India
*Corresponding Author: srinivasr343@gmail.com

Abstract

Residual stress is an inevitable problem and happens during any industrialized process and repair, while it is undesirable and it becomes necessary to examine the life of a component or workpieces. The present study is concentrated on the approximation of the residual stress at different regions of the welded specimen after its fabrication and to determine the residual stresses X-Ray diffraction (XRD) technique is used. In the present study, the main objective of the present study is to know whether the compressive and tensile stresses are induced in different weld shape specimens at the region of base metal, heat affected zone, and fusion zone area at two different positions of various weld bead shapes. Residual Stress measurement is conducted on the plane surface by examining the residual stresses and hardness of welded specimens it is identified that the convex specimen is found to exhibit good compressive residual stresses at all regions of the welded specimen and with less tensile residual stress at Heat affected zone.

Keywords: Cruciform shape welded joints, Heat affected zone, Residual stress, $\sin^2\psi$ method, X-Ray diffraction.

1. Introduction

Residual stress has an important role in the application of manufacturing components and mainly occur when there are variances in thermal expansion of materials, stiffness and yield stress during welding process [1, 2]. Majorly in the welding components, the residual stresses are produced due to the distinct contractions and due to immediate solidification of the welded portion and analysed that residual stress is minimized with help of heat treatment process [3]. The significance of weld deposit shrinkage and size plays the main role in obtaining the compressive or tensile stress value and by optimizing the welding parameters also able to reduce the amount of deformation [4].

Bahadur et al. [5] explained that there are various approaches to measure the residual stress those are XRD method, hole drilling method and ultrasonic method and suggested that non-destructive technique is preferable. According to Totten et al. [6], by using FEM method it is observed that concentration of residual stresses at weld region in the transverse position of weld specimen are very high, and the main reason is due to the part of specimen was close to the weld region and distort under less load. The numerical results obtained indicate that the superior residual stresses were distributed in the fusion zone and heat-affected zone [7]. A residual stress is a significant parameter while we are designing the machine elements or structural parts. The fatigue life of the welded specimens is reduced because of the occurrence of residual stresses during the fabrication process and stress concentration effect [8].

Residual stress produced in the welding process usually has a damaging effect on the mechanical properties of structural elements and can buckle the shape of parts. Stresses in titanium alloys remain the effect of the thermal gradients and the related change in microstructure produced. Though, the stress distribution is more difficult to forecast because of the complexity involved in metallurgical, thermal and mechanical phenomena [9]. Distribution of the residual Stresses were identified as similar in the Ti-6Al-4V laser beam joints and TIG weld joints [10-12] and it is confirmed that the maximum residual stresses are identified in the Heat Affected Zone of welds due to laser beam around 100 MPa, which are very lower when compared with the specimens, which undergo tungsten inert gas welding.

Withers et al. [13] proposed that residual stress occurs inside a component when there is no external load applied to it and need to find with external sources and Reddy [14] observed that residual stress can be originated because of metallurgical and mechanical process. Type I is the stress that exists in the component greater than the grain size of the material and type I stress origin from misfit that exist from nitriding, peening, cold hole expansion and welding. This stress can be found in plastically deformed materials, for an example in shot-peened surface and welded materials. Type II is the stress that varies with the scale of individual grain.

There are two common stresses present in residual stress, which are compressive stress and tensile stress. Both residual stresses depend on the location and type of uneven volumetric change taking place due to thermal (heat treatment and welding). Tensile residual stresses on surface normally harmful and can cause a brittle fracture, however, compressive residual stress at the surface normally will increase fatigue strength.

It is identified that the compressive residual stress at Heat Affect Zone region and at base metal are high and less amount of tensile residual stresses occurred at

the centre line of weld region [15]. From previous studies and research by Monin et al. [16], it is observed that tensile residual stress occurs in the weld metal zone and HAZ, whereas, compressive residual stress mostly concentrated in the base metal region. This phenomenon indicates that both residual stresses can exist in welded components. However, few studies say that tensile residual stress not only occurs at weld metal but exist at other regions also, compressive residual stress occurs not only at base metal and HAZ but also exist at weld metal zone. In this paper, analysis of residual stresses for different weld bead shapes of Ti-6Al-4V cruciform shape joints and hardness values were investigated at different regions of specimens.

2. Material and Methods

2.1. Material

Ti-6Al-4V alloy has important characteristics such as high strength to weight ratio, excellent corrosion resistance, good toughness, low thermal expansion rate, high temperature creep resistance and good formability and having the higher specific strength than most metals in temperatures below 500 °C. Ti-6Al-4V is an $\alpha+\beta$ alloy, which combines attractive mechanical properties with good workability and the best weldability of $\alpha+\beta$ alloys. To find hardness and residual stresses TI6AL4V material is considered with different weld bead shapes.

2.2. XRD technique

The $\sin^2\omega$ method of XRD is appropriate for plane stress situation and thus, it is used to find out the amount of the residual stress to the depth of around 20 micrometres in the welded component. The XRD method is used for measurement of lattice strain, which depends on well-established Bragg's law. If the availability of more residual stresses exists inside the sample, then the *d*-spacing will be unlike than that of an undisturbed state. This variance is proportional to the residual stress magnitude; the residual stress measurement of specimens is shown in Fig. 1.

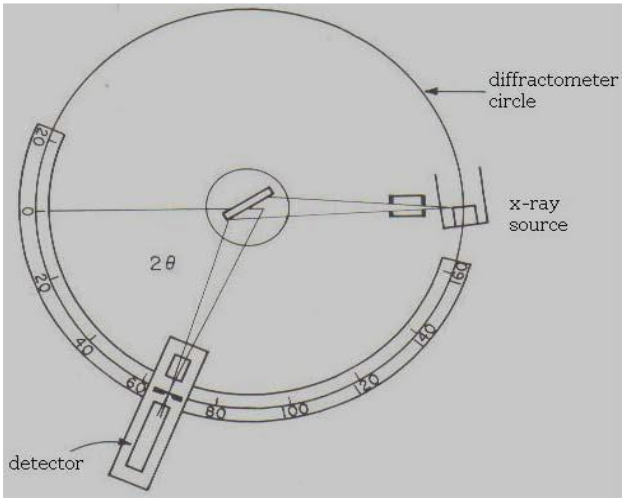

Fig. 1. Schematic diagram of X-ray diffractometer.

The crystal lattice is represented with normal three-dimensional allocations of the various number of atoms. In the crystal, the organization of atoms is in the form of parallel planes, which are spaced with distance-*d*. At the point, a monochromatic X-ray beam of wavelength λ is incident on crystals lattice planes at an angle θ. In this manner, the diffraction happens when the distance moved by the rays will be reflected after successive planes vary by wavelengths and are communicated by Bragg's law. Diffracted X-rays are gathered by the detector at various Bragg angles of 2θ. Stress distribution of material or specimen atomic lattice spacing is shown in Fig. 2.

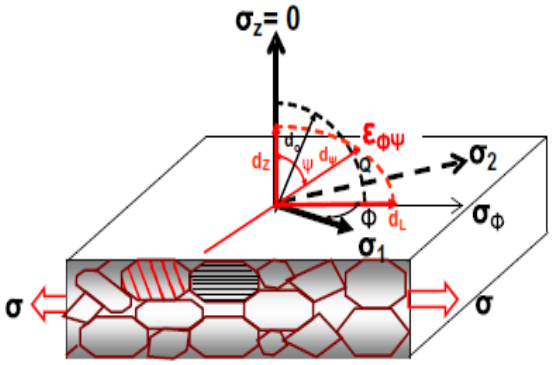

Fig. 2. Diagram of change in interatomic lattice spacing.

The X-ray diffraction technique is used to determine residual stresses in the weldment. The plot of the intensity of radiation against Bragg angle 2θ and the Gaussian curve fitting was done for the determination of the peak value of Bragg angle at each measurement location. The plot of lattice spacing (see Eq. (1)) against $\sin^2\psi$ (the tilt angle) and the determination of the slope of the curve from which, stress was calculated were all done with croto software.

$$\lambda = 2d\sin\theta \tag{1}$$

$$\varepsilon_x = \varepsilon_y = -\nu\varepsilon = \frac{-\nu\sigma_y}{E} \tag{2}$$

At the nearby surface of the material, X-ray measurement is carried out where $\sigma_z = 0$ and the strain, which is corresponding to the stress is calculated from Eq. (3).

$$\varepsilon_{\varphi\varphi} = \frac{1+\nu}{E}(\sigma_1\cos^2\varphi + \sigma_2\sin^2\varphi)\sin^2\psi - \frac{\nu}{E}(\sigma_1+\sigma_2) \tag{3}$$

$$\varepsilon_z = -\nu(\varepsilon_{x'} + \varepsilon_y) = \frac{-\nu}{E}(\sigma_x + \sigma_y) \tag{4}$$

$$\sigma_\phi = E/(1+\nu)\sin^2\psi\left(\frac{d_\psi - d_n}{d_n}\right) \tag{5}$$

$$\sigma_\phi = \left(\frac{E}{1+\nu}\right)m \tag{6}$$

2.3. Preparation of specimens

The primary joint structure is attained by securing the proportions of flange plate or main plate (100 mm × 24 mm × 6 mm) and cross plate (100 × 24 mm × 6 mm) in a cruciform position by using TIG welding as shown in Fig. 3. Subsequently, the fillets are made between the flange plate and cross plate by location of weld metal. TIG welding processes is preferred to prepare the joint and multi-pass welding procedures were employed to get the different weld bead shapes. Chemical properties and annealed mechanical properties are shown in Tables 1 and 2 respectively.

Table 1. Chemical composition of Ti-6Al-4V (Gr 5).

Ti-6Al-4V grade 5 chemical composition in weight percent								
Elements	**Ti**	**Al**	**V**	**Fe**	**H**	**N**	**0**	**C**
(wt%)	**89.3**	**5.9**	**3.8**	**0.44**	**0.017**	**0.06**	**0.26**	**0.08**

Table 2. Mechanical properties of Ti-6Al-4V (Gr 5).

Tensile strength	Yield strength	Poisson's ratio	Elastic modulus	Shear modulus	Elongation at break
895 MPa	**750MPa**	**0.31**	**112 GPa**	**42 GPa**	**14%**

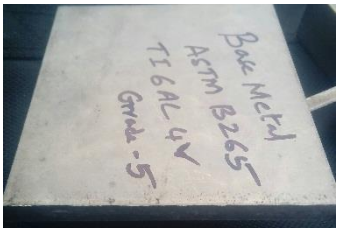

(a) Base metal.

(b) TIG welding.

(c) Convex specimen.

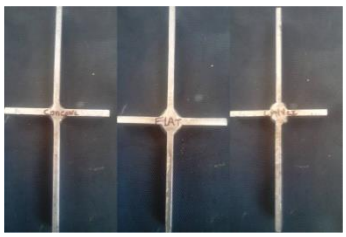

(d) Various weld bead shape joints.

Fig. 3. Preparation of cruciform shape welded joints of Ti-6Al-4V.

3. Experiment procedure

3.1. Measurement of residual stresses using XRD equipment

Surface Residual stress is estimated by the XRD technique, and the compressive stress and measurement of residual stress is executed in a PORTABLE ANALYSER XSTRESS3000, which as 1 mm collimator (25 kV, 4 mA), utilizing

the $\sin^2\psi$ method for measuring the lattice space d of material at 5 different positions of ψ-angles between -45º and +45º. In view of Bragg's law, using CrKα radiation (λCrkα = 1.542 Å) diffracting the (211) plane for ferrite phase at 2θ = 148.69°. With the help of on a regression fit, the distinctions of 2θ versus $\sin^2\psi$ plots are confirmed and the residual stress is estimated. A precision of around 15MPa was accomplished by methods for X-beam diffraction. Specifications of XRD instrument is shown in Table 3. Different weld bead shapes specimens are experimentally investigated in horizontal (position 1) to determine the Residual stresses as shown in Fig. 4.

The XRD is best-developed approaches, which is accessible for estimation of residual stress. It is an NDT technique and uses the distance between (*d*-spacing) as a strain gauge. This method is applicable to polycrystalline, semi-crystalline and materials crystalline, if the material is under tension, the *d*-spacing increase and whereas the material is in compression, the *d*-spacing is going to decrease. Among the samples, concave, flat and convex, which are having negative values and positive values of residual stresses at different regions or zones are to be studied.

Table 3. Specifications of XRD equipment.

Material	Ti-ALPHA (Cu_Ka) 1 (HCP, hkl-302)
Tube	Cu_K-Alpha
Wavelength	1.542 A°
X-ray voltage	25 kV
X-ray current	4 mA
Expected time:	20
Number of experiments	10
Aperture	2 mm
Filters	Nil

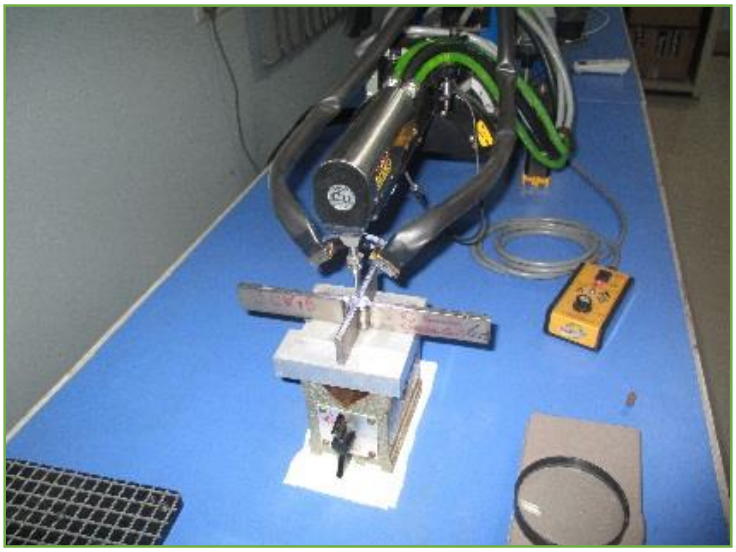

Fig. 4. Specimen placed in horizontal (position 1).

Residual stress is measured at various positions on the different weld bead shapes at fusion zone, along HAZ and BM region. Figures 5(a) and (b) shows that measurement of residual stress for the cruciform welded specimen of 6 mm thickness of different weld bead shapes in position 2, i.e., specimens placed in vertical.

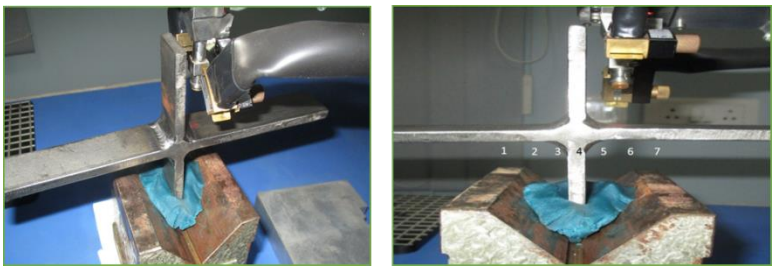

(a) Front view. **(b) Side view.**

Fig. 5. Measurement of residual stresses when cruciform welded specimens when placed vertical (position 2).

3.2. Microhardness studies

Hardness is the measure of the resistance offered by the material for the local compressive load and measured with Vickers hardness equipment as shown in

Figure 6(a) consists of a diamond indenter, in the form of a right pyramid shape with a square base and angle between the opposite faces is 136^0. The indentation is shown in Fig. 6(b). For calculating Vickers Hardness Value (HV), the distance between diagonal corners has to be measured. The Vickers hardness number is the ratio of the load applied in kg to the area of the sloping surface of indentation in square mm.

(a) Specimens positioned in Vickers hardness equipment.

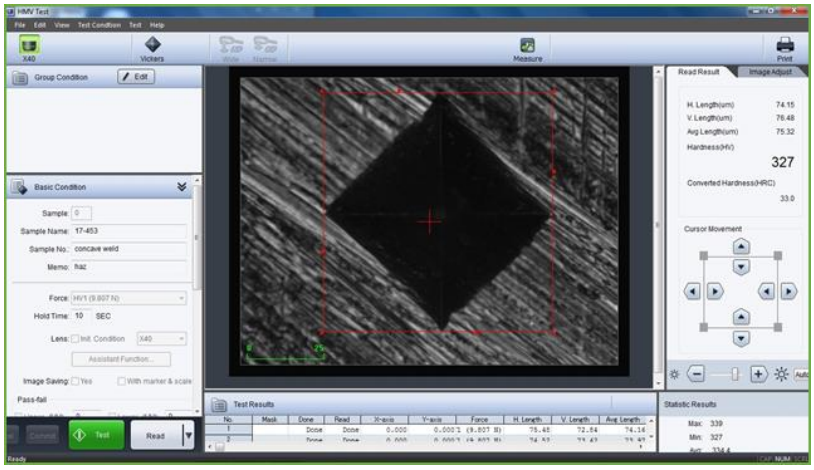

(b) Image of indentation.

Fig. 6. Vickers hardness equipment and indentation.

4. Results and Discussion

XRD measurement is done, and numerous investigations made at various tilt angles, ω, and the plot of lattice spacings is based on the calculation from Eq. (1) against $\sin^2\omega$ is shown in Fig. 7. In position 1, maximum compressive stress is observed for the convex shape specimen.

Minimum compressive stresses are induced in convex shape specimen when compared to other two shapes in position 2 the stress values of convex shape reveals that, the strength of the joint along the weld is having more compressive stress and high strength when compared with the specimen across the weld.

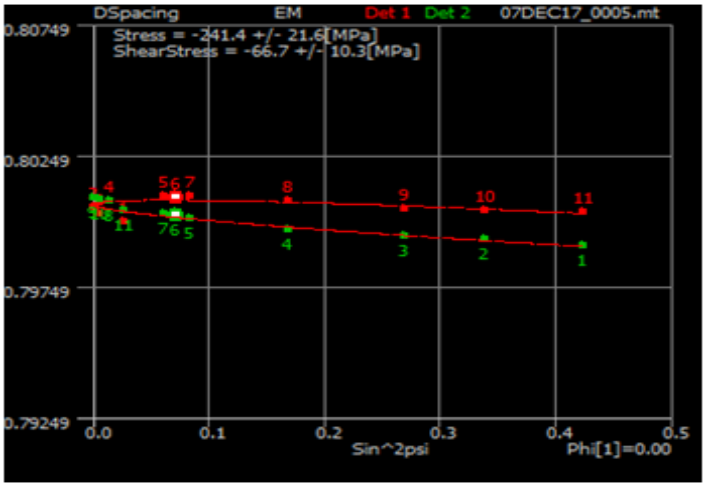

(a) Concave specimen.

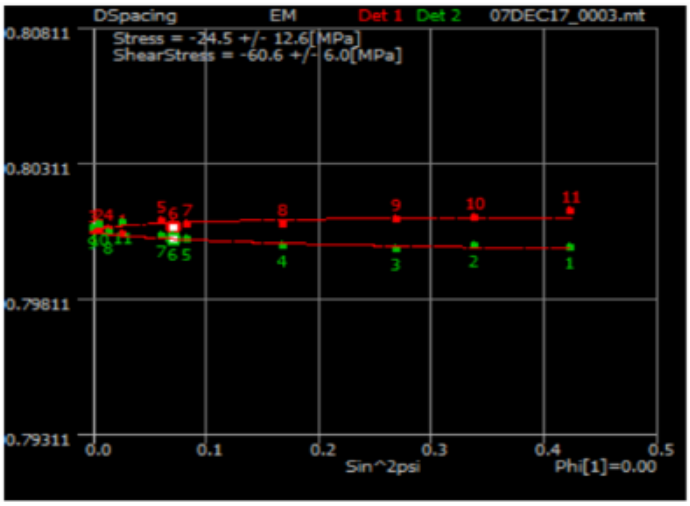

(b) Convex specimen.

Fig. 7. Linear dependence of lattice spacing of reflection upon $\sin^2\omega$.

Tables 4 to 7 shows the values obtained from the experiment procedure are calculated using $\sin^2\omega$ method for concave shape, convex shape and flat weld bead shape specimen. There will be two tilts in goniometer, for every point on the welded specimen two values should be measured. Detectors 1 and 2 will tilt in opposite directions.

A linear graph of $\sin^2\psi_{vs}$ *d*-spacing is fitted to diffraction data with a near to positive slope of a concave specimen and negative slope of a convex specimen.

Tables 4 and 5 shows that measurements of residual stress for convex specimen, where Beta angles are varied from +25 to -25 and values of different parameters will be in reverse order for two tables and more intensity is observed for detector 1 of XRD equipment for convex specimen, the importance of more intensity values gives high residual stress in compressive, which will give more strength to weld strength.

Table 4. Residual stress measurement is conducted by X-Ray diffraction for convex specimen (detector-1).

Beta angles	Psi	Sin^2psi	*d*-spacing	2 Theta	Strain*E3	FWHM	Breadth	Intensity
25	0.35	0.0264	0.800445	148.78	-0.217	3.778	4.23	522.88
19.99	4.33	0.0057	0.800642	148.68	0.029	3.657	4	503.26
15.66	0	0	0.800609	148.69	-0.012	3.811	4.31	505.57
8.68	-6.98	0.0148	0.800663	148.67	0.055	3.506	3.96	547.71
1.28	14.37	0.0616	0.800918	148.54	0.374	3.63	4.15	532.84
0	-15.65	0.0728	0.800717	148.64	0.122	3.371	3.86	587.42
-1.28	-16.94	0.0849	0.800796	148.6	0.221	3.332	3.6	552.16
-8.68	-24.33	0.1698	0.800847	148.57	0.285	3.602	4.15	577.74
-15.66	-31.31	0.2701	0.801022	148.49	0.503	3.763	4.09	529.84
-19.99	-35.64	0.3396	0.801091	148.45	0.589	3.877	4.43	486.78
-25	-40.65	0.4245	0.80129	148.35	0.839	4.091	4.58	446.78

Table 5. Residual stress measurement is conducted by X-Ray diffraction for convex specimen (detector-2).

Beta angles	Psi	Sin^2psi	*d*-spacing	2 Theta	Strain*E3	FWHM	Breadth	Intensity
25	40.65	0.4245	0.799974	149.02	-0.805	3.776	4.17	369.12
19.99	35.64	0.3396	0.800014	149	-0.755	3.623	3.83	400.05
15.66	31.31	0.2701	0.799931	149.04	-0.859	3.276	3.45	452.37
8.68	24.33	0.1698	0.800037	148.99	-0.726	3.565	3.81	453.32
1.28	16.94	0.0849	0.800293	148.86	-0.407	3.422	3.67	441.25
0	15.65	0.0728	0.800295	148.86	-0.404	3.188	3.24	449.7
-1.28	14.37	0.0616	0.800373	148.82	-0.307	3.372	3.45	461.7
-8.68	6.98	0.0148	0.80052	148.74	-0.123	3.485	3.79	399.25
-15.66	0	0	0.800723	148.64	0.13	3.614	3.9	382.27
-19.99	-4.33	0.0057	0.800825	148.58	0.258	3.724	3.99	387.73
-25	-9.35	0.0264	0.800903	148.55	0.355	3.669	3.94	381.34

From Tables 6 and 7, the intensity values are related and identified that both detector 1 and detector 2 gives almost similar values when compared with convex specimen intensity values and shows that concentration of residual stresses is uniformly distributed. Intensity values, which are recorded in Tables 4 to 7 are obtained from the Figs. 8 and 9.

Strain values of detector 1 are more when compared to detector 2 and intensity is maximum for detector 1 and scattering angles.

Table 6. Residual stress measurement is conducted by X-ray diffraction for concave specimen (detector-1).

Beta angles	Psi	Sin^2psi	*d*-spacing	2 Theta	Strain*E3	FWHM	Breadth	Intensity
25.00	9.35	0.0264	0.799979	149.02	-0.799	2.424	2.83	1026.50
19.99	4.33	0.0057	0.800261	148.87	-0.447	2.460	2.82	626.77
15.66	0.00	0.0000	0.800519	148.74	-0.125	2.445	2.79	438.48
8.68	-6.98	0.0148	0.800771	148.61	0.191	2.315	2.75	395.84
1.28	-14.37	0.0616	0.800936	148.53	0.396	2.316	2.80	401.05
0.00	-15.65	0.0728	0.800865	148.56	0.308	2.363	2.81	430.43
-1.28	-16.94	0.0849	0.800914	148.54	0.369	2.107	2.65	498.86
-8.68	-24.33	0.1698	0.800729	148.63	0.138	1.977	2.43	963.32
-15.66	-31.31	0.2701	0.800460	148.77	-0.198	1.934	2.33	1564.08
-19.99	-35.64	0.3396	0.800379	148.81	-0.300	1.924	2.26	1763.15
-25.00	-40.65	0.4245	0.800299	148.85	-0.400	1.986	2.43	1595.34

Table 7. Residual Stress measurement is conducted by XRD for concave specimen (detector 2).

Beta angles	Psi	Sin^2psi	*d*-spacing	2 Theta	Strain*E3	FWHM	Breadth	Intensity
25.00	40.65	0.4245	0.799036	149.51	-1.977	2.026	2.29	323.89
19.99	35.64	0.3396	0.799307	149.37	-1.638	1.991	2.26	466.98
15.66	31.31	0.2701	0.799422	149.31	-1.495	1.995	2.28	674.85
8.68	24.33	0.1698	0.799625	149.20	-1.242	1.916	2.18	1207.12
1.28	16.94	0.0849	0.800099	148.96	-0.649	2.014	2.30	1536.01
0.00	15.65	0.0728	0.800189	148.91	-0.537	2.017	2.30	1552.58
-1.28	14.37	0.0616	0.800277	148.87	-0.427	2.010	2.25	1521.12
-8.68	6.98	0.0148	0.800737	148.63	0.147	2.011	2.25	997.48
-15.66	-0.00	0.0000	0.800873	148.56	0.317	2.157	2.35	443.47
-19.99	-4.33	0.0057	0.800784	148.61	0.206	2.177	2.26	300.47
-25.00	-9.35	0.0264	0.800398	148.80	-0.276	2.217	2.31	215.31

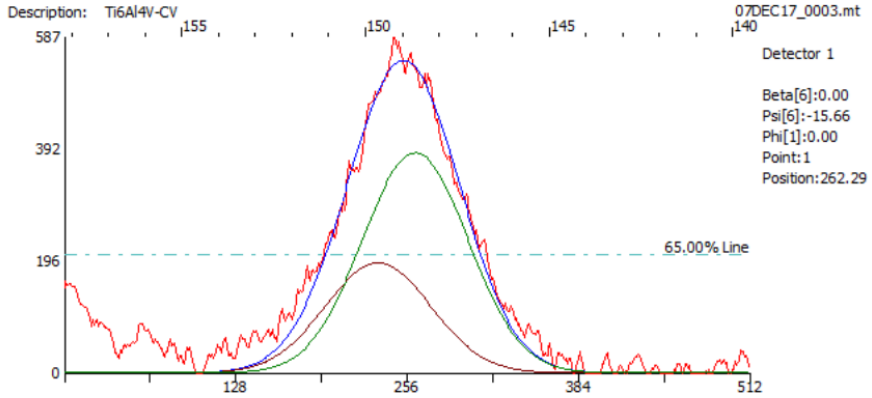

(a) Detector-1 peak values.

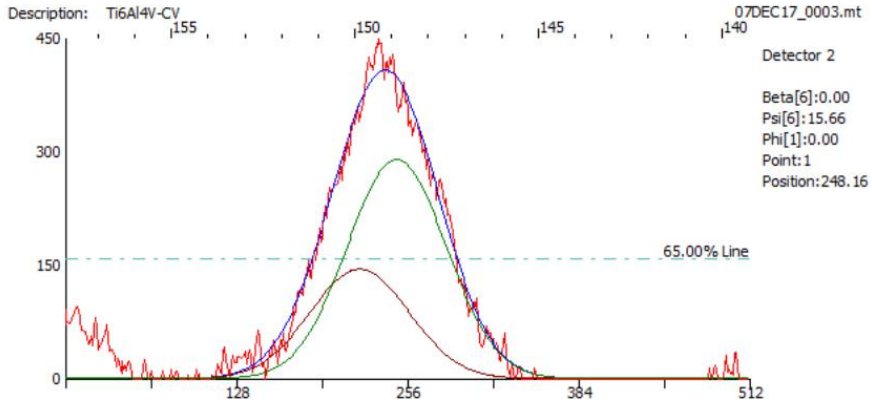

(b) Detector-2 peak values.

Fig. 8. Two peak values of scattering angle θ are given together with the corresponding *d*-spacing values for detector 1 and detector 2 (convex specimens).

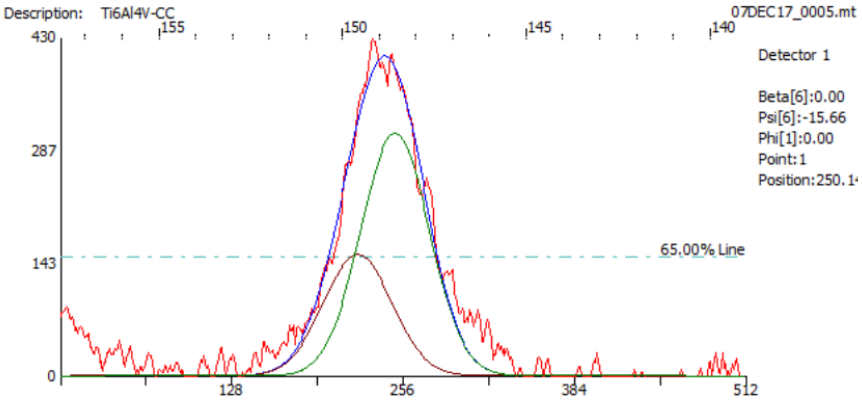

(a) Detector 1 peak values.

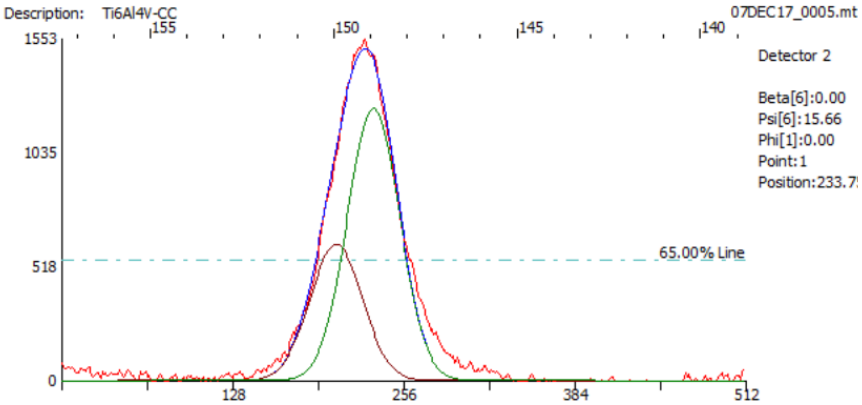

(b) Detector 2 peak values.

Fig. 9. Two peak values of scattering angle θ are given together with corresponding *d*-spacing values for detectors 1 and 2 (concave specimens).

Values obtained in Table 4-7 shows that results obtained from XRD testing equipment help to know the slope between $\sin^2\psi$ and *d*-spacing. If negative slope occurs it indicates compressive residual stresses are induced and positive slope occurs it shows tensile residual stress. Figures 7(a) and b represents residual stress values of convex shape specimen and concave shape at heat affected zone.

The existence of residual stress in the material, which is examined by XRD equipment produces a shift in angular position at peak value, which is directly measured by the detector. In Fig. 5, the shift in the peak positions is observed for different samples. It is significant to attain a diffraction peak of suitable intensity values. The peaks must be free of interference from adjacent peaks and therefore, the Bragg angle (2θ) can be estimated experimentally and the *d*-spacing is, therefore, calculated using Bragg's law.

One of the major difficulties with XRD is the limitation imposed on the test piece geometry and size. The geometry has to be such that an X-ray can both hit the measurement area and still be diffracted to the detector without hitting any obstacles. However, due to the irregular geometry of some of the samples, it is not possible to get clear diffraction data.

Residual stresses are examined in joints on position 1, i.e., longitudinal (L) and position 2, i.e., transversal (T) direction of the weld bead. These measurements are made in three different zones, fusion zone (FZ), base metal (BM) and heat-affected zone (HAZ). The stress is theoretically calculated from the gradient and diffraction elastic constant of the material. Lattice spacing is $d = i_n$, as d is known as the intercept and represented with the y-axis when $\sin^2\omega = 0$, from the slope 'm' and the stress is thus, considered from Eq. (6).

Portable X-ray stress analyzer is used for residual stress measurement and goniometer with back reflection type having a 2θ range from 140° to 170° consists parallel beam geometry and XRD intensity profiles at various measurement locations are attained at different ψ angles, from the slope of $\sin^2\psi$ vs peak 2θ, the residual stresses are determined depending on equation 1. The values of 2θ are peak and obtained at various ψ values, where v and E denote the Poisson's ratio, Young's modulus.

4.1. Intensity results

The residual stress in position 1 are higher than the stresses in position 2 in the direction longitudinal, maximum tensile stress is observed in the centreline of the weld bead and compressive stress is identified at high in the position 2. The transversal residual stress is usually of tensile stress type in the FZ and HAZ, however, in transversal cross-sections near the beginning and the end of the fusion line, compressive stresses are induced. Residual stress obtained for position 1 is shown in Table 8. It is observed that convex specimen attains more compressive residual stresses, in all regions of the specimen.

Table 8. Residual stress (MPa) values carried out on welded specimens for position 1.

Region	Distance from weld centre(mm)	Concave	Convex	Flat
BM	-16	-298	-310	-285
BM	-12	-215	-237	-225
FZ	-8	-112	-165	-135
FZ	-4	-53	-75	-67
HAZ	0	60	-24	25
FZ	4	-58	-85	-72
FZ	8	-120	-170	-145
BM	12	-220	-245	-298
BM	16	-287	-302	-295

In position 1, compressive type (-165 MPa to −53 MPa) residual stress is induced in the FZ and at the base metal region, the stresses are varied from (-310 MPa to -230 MPa). Whereas, the HAZ zone the residual stresses observed are in range (+60 MPa to -24 MPa). In previous studies, butt welded joints tensile stresses are induced at fusion zone region, whereas cruciform welded joint is having compressive stresses, in which, having more strength compared to butt welded joint.

In position 2, significant tensile residual stress (+115 MPa) produced for the concave specimen is initiated in the fusion zone. Tensile residual stresses with magnitude (+43 MPa to +115 MPa) exist in the fusion zone for all specimens. The

compressive stresses are induced at heat affect zone varying from (-75 MPa to -225 MPa). Residual stress obtained for position 2 is shown in Table 9.

From Table 9, it is observed that concave specimen is holding high compressive stress at the base metal region, however, unfortunately, at fusion zone high tensile stresses, this leads to failure of the joint at fusion zone. For convex specimen the tensile residual stresses are less when compared to concave and flat weld shape, after determination of residual stresses at both positions, a convex specimen is having good intensity values, high compressive residual stresses and minimum tensile residual stress, which improves the strength of a material.

Figures 10 and 11 show residual stress is completely distributed in the compressive residual stress region towards the base metal and fusion region, however, tensile residual stresses are detected in the heat-affected zone for position 1 whereas, distribution of compressive residual stress at the regions of base metal and HAZ is concentrated and tensile residual stresses are at the fusion zone region and one more observation is that the stress is linearly increasing towards tensile region across the weld bead in both the positions. The stress distribution is almost equal on either side of the fusion zone because of the consistency of welding parameters.

Table 9. Residual stress (MPa) values carried out on welded specimens for position 2.

Region	Distance from weld centre	Concave	Convex	Flat
BM	-12	-320	-264	-315
BM	-8	-265	-172	-235
HAZ	-4	-225	-83	-177
FZ	0	115	43	74
HAZ	4	-195	-75	-163
BM	8	-241	-185	-245
BM	12	-310	-250	-305

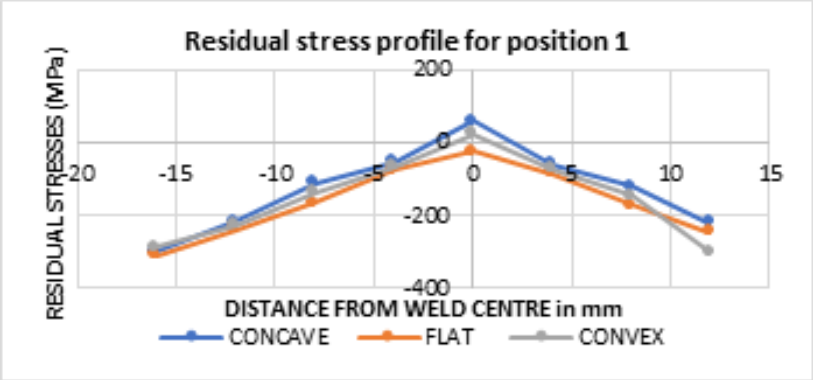

Fig. 10. Residual stress distribution at surface of different welded specimen in position 1.

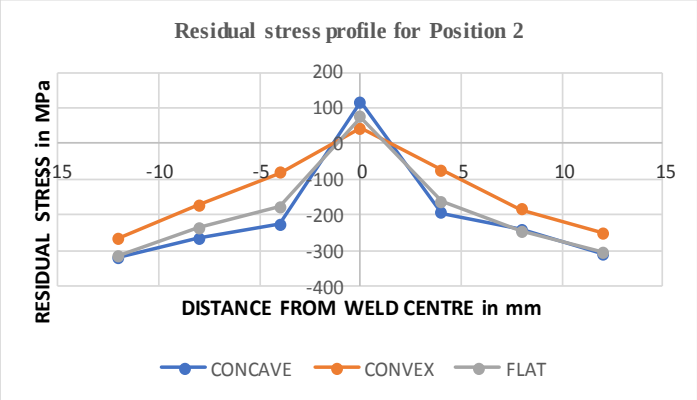

Fig. 11. Residual stress distribution at the surface of different welded specimen in position 2.

Once the weld metal is reached to the liquid state phase, the expansion of the molten metal is controlled by colder parent material and therefore, greater yield strength will result in plastic deformation in high temperature at the weld metal region. However, after the welding process, the specimens are tested under room temperature in the regions of weldment and HAZ will contracts as the temperature lowers, however, the contraction in the weld and HAZ is restrained by the colder parent material, therefore, causing tension in the HAZ and the weld metal. The residual tensile stress is induced more in the weld metal region and HAZ, whereas, compressive residual stress is concentrated near the parent material or base metal region.

By considering the experiment values of d-spacing and $\sin^2 \psi$ of position 1 and position 2 and can able to determine the compressive stresses. A negative slope indicates that the residual stresses are in compressive and whereas, positive slope represents the stresses induced are tensile, Fig. 12 shows the negative slope is obtained for the concave specimen at HAZ zone of the specimen.

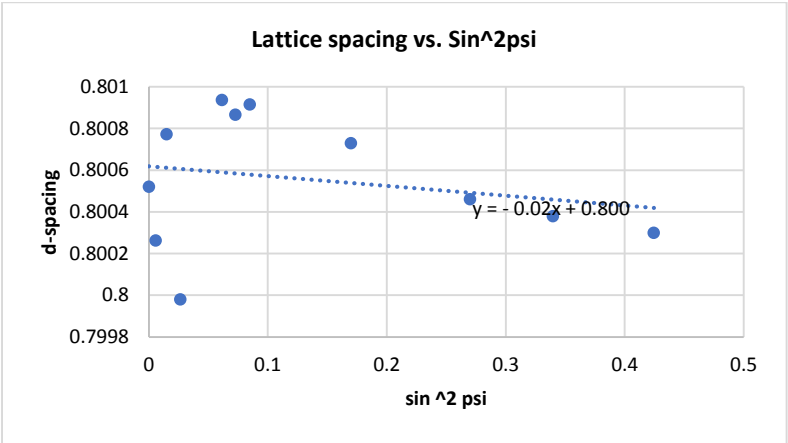

Fig. 12. Slope obtained from experimental values.

4.2. Microhardness values of different weld bead shape specimens

The Vickers method depends upon microhardness test and macro analysis of specimen using optical measurement system, a range of loads are used with help of diamond indenter to make an indentation and to obtain a hardness value for measuring Vickers hardness. Microhardness tester is used (Shimadzu Model: HMV-G) as per ASTM E 340-15 and IS: 1501-13. Balasubramanian et al. [17] reported that the test is performed at a load of 0.5 kg and readings are taken at regular intervals on both sides of the regions. The microstructure of the welded specimen is observed, using an optical microscope. A minimum of five indentation diameters is used as the distance between the measurements. The hardness profiles presented are an average of 3 profiles across the welds at different depths as shown in Fig. 13.

The value of micro-hardness for the base material of Ti-6Al-4V is nearer to 339 ± 2.1 HV. The change in the hardness is less at the BM area for the as-welded specimen, while there is a small decrease in the hardness of the BM area after welding. It is observed that the hardness of the FZ and HAZ of the cruciform welded Ti-6Al-4V concave shape is around 365 ± 4 HV and 334 ± 5 HV and hardness of the FZ and HAZ of the convex shape is around 438 ± 5 HV and 359 ± 6 HV. HAZ and FZ of the flat shape are around 259 ± 3 HV and 280 ± 3 HV. Microhardness values are shown in Table 9.

For convex shape specimen, tensile residual stress values are more and the compressive residual stress values are less when compared to concave shape and flat shape in position 2.

In previous studies, it is discussed that more compressive stress will give more strength to the welded joint. If the compressive residual stress value is high and tensile residual stress is less than the strength of weld specimen is predicted to be high. The hardness value, which is determined from Vicker hardness test reveals that maximum values are recorded for concave shape specimen at all regions, however, the residual stresses obtained for concave shape specimen are not correlated with the hardness value.

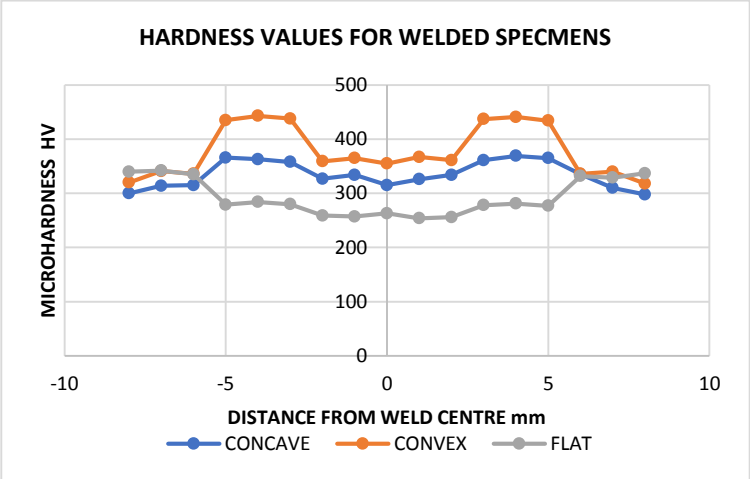

Fig. 13. Distribution of hardness values for different welded specimens.

Table 9. Micro hardness values of Ti-6Al-4V of different weld bead shapes at different zones.

	Distance from weld centre in mm	Concave weld specimen	Convex weld specimen	Flat weld specimen
BM	-8	300	320	340
	-7	314	341	342
	-6	315	336	335
	-5	366	435	279
HAZ	-4	363	443	284
	-3	358	438	280
	-2	327	359	259
FZ	-1	334	365	257
	0	315	355	263
	1	326	367	254
HAZ	2	334	361	256
	3	361	437	278
	4	369	441	281
BM	5	365	434	277
	6	335	336	332
	7	310	340	329
	8	298	318	337

5. Conclusions

Ti-6Al-4V welded joints were evaluated to know the hardness of different weld beads at different zones and identified the impact on strength of the weld joint. XRD equipment determined the residual stress at different weld regions of various weld bead shape specimens and reveals the importance of compressive residual stress and tensile residual stress:

- Experimental investigation on Ti-6Al-4V on cruciform weld joints using XRD technique reveals that in position 2, maximum residual tensile stresses are at fusion zone of a concave specimen when compared with convex and flat shape specimens. At base metal and heat affect zone, compressive residual stresses are varied.
- In position 1, at heat affect zone the tensile residual stresses value is observed for concave shape specimen whereas compressive residual stress is identified for other zones at BM, FZ. Results obtained for cruciform shape welded joint is converse to the butt weld joints. Vickers hardness measurements found that convex specimens are having more hardness values.
- Both residual stress and hardness values of various weld bead shapes are analysed at various zones.

Nomenclatures

d	Lattice spacing
m	Slope

Greek Symbols

E	Young modulus
2θ	Bragg angle

λ	Wavelength
ν	Poisson's ratio
φ	Angle of rotation
ψ	Psi
ω	Omega

Abbreviations

FWHM	Full Width at Half Maximum
FZ	Fusion Zone
HAZ	Heat Affected Zone
HV	Vickers Pyramid Number
ND	Neutron Diffraction Method
RS	Residual Stress
XRD	X-Ray Diffraction Method

References

1. Withers, P.J.; and Bhadeshia, H.K.D.H. (2001). Residual stress – Part I - Measurement techniques. *Materials Science and Technology*, 17(4), 355-365.
2. Withers, P.J.; and Bhadeshia, H.K.D.H. (2001). Residual stress – Part II - Nature and origins. *Materials Science and Technology*, 17(4), 366-375.
3. Sedek, P.; Brozda, J.; Wang, L.; and Withers, P.J. (2003). Residual stress relief in MAG welded joints of dissimilar steels. *International Journal of Pressure Vessels and Piping*, 80(10), 705-713.
4. Cheng, X.; Fisher, J.W.; Prask, H.J.; Gnaupel-Herold, T.; Yen, B.T.; and Roy, S. (2003). Residual stress modification by post weld treatment and its beneficial effect on fatigue strength of welded structures. *International Journal of Fatigue*, 25(9-11), 1259-1269.
5. Bahadur, A.; Kumar, B.R.; Kumar, A.S.; Sarkar, G.G.; and Rao, J.S. (2004). Development and comparison of residual stress measurement on welds by various methods. *Materials Science and Technology*, 20(2), 261-269.
6. Totten, G.; Howes, M.; and Inoue, T. (2002). *Handbook of residual stress and deformation of steel.* Ohio, United States America: ASM International.
7. Kassab, R.K.; Champliaud, H.; Le, N.V.; Lanteigne, J.; and Thomas, M. (2012). Experimental and finite element analysis of a t-joint welding. *Journal of Mechanical Engineering and Automation*, 2, 411-421.
8. Abid, M.; and Qarni, M.J. (2009). 3D thermal finite element analysis of single pass girth welded low carbon steel pipe-flange joints. *Turkish Journal of Engineering Environmental Sciences*, 33(4), 281-293.
9. Zhang, J.X.; Xue, Y.; and Gong, S.L. (2005). Residual welding stresses in laser beam and tungsten inert gas weldments of titanium alloy. *Science and. Technology of Welding and Joining*, 10(6), 643-646.
10. Noyan, I.C.; and Cohen, J.B. (1987). *Residual stress: Measurement by diffraction and interpretation*. New York, United States of America: Springer-Verlag.
11. Cullity, B.D.; and Stock, S.R. (2001). *Elements of X-ray diffraction* (3rd ed.), Essex, England: Pearson Education Limited

12. Dias, J.S.; Chuvas, T.C.; and Fonseka, M.d.P.C. (2016). Evaluation of residual stresses and mechanical properties of if steel welded joints by laser and plasma processes. *Materials Research*, 19(3), 721-727
13. Withers, P.J.; Turski, M.; Edwards, L.; Bouchard; P.J.; and Buttle, D.J. (2008). Recent advances in residual stress measurement. *International Journal of Pressure Vessels and Piping*, 85(3), 118-127.
14. Reddy, A.V. (2004). *Investigation of aeronautical and engineering component failure* (1st ed.). Florida, United States of America: CRC Press LLC.
15. Ju, J.-B.; Lee, J.-S.; Jang, J.-i.; Kim, W.-s.; and Kwon, D. (2003). Determination of welding residual stress distribution in API X65 pipeline using a modified magnetic Barkhausen noise method. *International Journal of Pressure Vessels and Piping*, 80(9), 641- 646.
16. Monin, V.I.; Gurova, T.; Castello, X; and Estefen, S.F. (2009). Analysis of residual stress state in welded steel plates by X-ray diffraction method. *Reviews on Advanced Materials Science*, 20(2), 172-175
17. Balasubramanian, M.; Ramesh, G.; and Balasubramanian, V. (2015). Diffusion bonding of titanium alloy Ti-6al-4v and AISI 304 stainless steel - an experimental investigation. *Journal of Engineering Science and Technology* (*JESTEC*), 10(10), 1342-1349